

# Prediction of Large Magnetic Moment Materials With Graph Neural Networks and Random Forests

Sékou-Oumar Kaba,<sup>1, 2,\*</sup> Benjamin Groleau-Paré,<sup>3</sup> Marc-Antoine Gauthier,<sup>3</sup> André-Marie Tremblay,<sup>3</sup> Simon Verret,<sup>1, 3</sup> and Chloé Gauvin-Ndiaye<sup>3</sup>

<sup>1</sup>*Mila - Quebec Artificial Intelligence Institute & IVADO - Institut de Valorisation des Données, Montréal, Québec, Canada H2S 3H1*

<sup>2</sup>*School of Computer Science, McGill University, Montréal, Québec, Canada H3A 0E9*

<sup>3</sup>*Département de physique & Institut Quantique, Université de Sherbrooke, Québec, Canada J1K 2R1*

(Dated: November 30, 2021)

Magnetic materials are crucial components of many technologies that could drive the ecological transition, including electric motors, wind turbine generators and magnetic refrigeration systems. Discovering materials with large magnetic moments is therefore an increasing priority. Here, using state-of-the-art machine learning methods, we scan the Inorganic Crystal Structure Database (ICSD) of hundreds of thousands of existing materials to find those that are ferromagnetic and have large magnetic moments. Crystal graph convolutional neural networks (CGCNN), materials graph network (MEGNet) and random forests are trained on the Materials Project database that contains the results of high-throughput DFT predictions. For random forests, we use a stochastic method to select nearly one hundred relevant descriptors based on chemical composition and crystal structure. This turns out to give results for the test sets that are comparable to those of neural networks. The comparison between these different machine learning approaches gives an estimate of the errors for our predictions on the ICSD database.

## I. INTRODUCTION

In recent years, materials informatics and statistical learning methods have been introduced in the search for materials with specific properties, such as high-temperature superconductors [1], photovoltaics [2], radiation detector materials [3] and metallic glasses [4]. These methods have the advantage of allowing to explore sets of materials that would be prohibitively large for conventional theoretical methods or experiments. Though traditional machine learning methods such as tree-based algorithms [5, 6], kernel methods [6, 7], support vector machines [6] and multilayer perceptrons [6] have shown some success in the prediction of magnetic properties, the frequent introduction of new large materials databases [8–11] has also enabled the development of sophisticated neural networks for this type of application. In particular, Graph Neural Networks algorithms (GNNs) have recently been shown to obtain state-of-the-art performance on benchmark tasks [12–14]. These methods have been shown to successfully predict formation energy, band gap and bulk modulus with error magnitudes similar to those of density functional theory (DFT) calculations, but have not yet been used for the study of magnetic properties.

Demand for strong permanent magnets for technological applications is rising [15]. This is closely related to the fact that many countries are looking to transition away from fossil fuels to more sustainable energy sources. Indeed, one of the main drivers of demand for permanent magnets is the production of motors for hy-

brid and electric vehicles, which are rapidly gaining popularity. Another growing application is wind turbine generators. For most applications,  $\text{Nd}_2\text{Fe}_{14}\text{B}$  is the material of choice. However, discovering rare earth free permanent magnets would be highly desirable for environmental and economic reasons.

Materials that have a large magnetic moment per mass unit, but that are not permanent magnets, still have multiple applications of interest. A promising application for such materials is magnetic refrigeration. Magnetic refrigeration is a technology based on the magnetocaloric effect, through which the temperature of a magnetic material varies with the adiabatic application of a magnetic field [16–18]. Because it requires the use of solid state materials instead of gaseous refrigerants, magnetic refrigeration is a more environmentally-friendly technology than traditional refrigeration. However, it requires ferromagnetic materials with a Curie temperature around room temperature that also have many specific properties, such as a low specific heat and a high electrical resistivity. The reference materials that exhibit a large magnetocaloric effect around room temperature are gadolinium and some Gd-based alloys like  $\text{Gd}_5\text{Si}_2\text{Ge}_2$  [19, 20]. These materials are expensive, which limits their commercial use, as well as metallic, which diminishes energy efficiency due to heat loss.

Often, the search for new materials that exhibit specific properties is done through trial and error, limiting the number of materials that can be studied both theoretically and experimentally. Considering the challenges that surround the design of new materials for magnetic refrigeration and other applications, we investigate the usefulness of machine learning for materials in the study of magnetic properties as a first step towards the discov-

\* kabaseko@mila.quebec

ery of new materials.

In this paper, we assess the performance of two recently proposed neural networks, CGCNN [12] and MEGNet [13], and compare it to that of the random forest, a statistical machine learning method [21–23], for the prediction of the magnetization of materials. To do so, we train our models on the Materials Project database, a DFT database frequently used as a training set in the field of machine learning for material properties [8]. We characterize the Materials Project dataset and describe a preprocessing scheme based on the energy above hull to reduce bias in its distribution of magnetic orders. Our work shows that neural networks are comparable to random forests for the prediction of magnetization. We then apply our trained models on the ICSD database, which contains around 100 000 stoichiometric experimentally-studied materials [24]. We discuss the suitability of the proposed materials for the specific application to magnetic refrigeration.

In the following section, we present the results of our study. We first describe the datasets used for training and inference. We then evaluate the accuracy of the trained models. This is followed by our predictions and error estimates of magnetic moment on real materials.

## II. RESULTS

We first discuss the Materials Project dataset that we use to train the models and then the ICSD database of materials that we use to make predictions. In subsection B, we present the setup for training and inference, in C we compare and evaluate the different methods, and we give our predictions in D.

### A. Datasets

#### 1. Materials Project

The training data used in this work comes from the Materials Project dataset (V2020.06) [8]. It is one of the largest datasets obtained from high-throughput DFT calculations and has become a standard in machine learning based materials studies.

Materials Project comprises stoichiometric crystalline materials, and provides their chemical composition, relaxed structures and a number of properties such as the formation energy, the energy above hull, the band structure and the spontaneous unit cell magnetization. To our knowledge, this last property in Materials Project has not been used yet for machine learning applications.

The Materials Project dataset is constructed using the Vienna Ab Initio Simulation Package (VASP) software [25] and the GGA functional. The calculations are done using the projector augmented wave pseudopotentials implemented in VASP. This method has the advantage of reducing computation time while retaining precision [26].

The initial crystal structures used as input for the calculations are obtained from the Inorganic Crystal Structure Database (ICSD), which we describe below. The calculations then allow for structure relaxation. All calculations are performed at  $T = 0$ , meaning that the dataset should contain the ground state properties of materials. No spin-orbit coupling effects are included. We note that all the calculations are initialized in the ferromagnetic configuration. Antiferromagnetic configurations can be reached in the crystal relaxation stage. However, it has been shown that this method favours ferromagnetic configurations, even when low-spin antiferromagnetic or ferrimagnetic configurations could have lower energies [27]. In 2019, a new workflow was introduced as an effort to include appropriate antiferromagnetic ground states and counter the ferromagnetic bias [27]. At this time, new ground-state calculations using this workflow were performed for about 520 materials, less than 2% of the Materials Project dataset.

The most difficult materials to simulate with DFT calculations are the ones in which electronic correlations are strong [28]. This is most notable in materials that contain  $d$  or  $f$  valence electrons, like the transition metals and the rare earths. These electrons are also the ones that participate in the magnetic properties. In the Materials Project dataset, all calculations on oxides containing Co, Cr, Fe, Mn, Mo, Ni, V and W atoms are performed with the GGA+U scheme that aims to better represent the electronic correlations. We still note that the magnetic ground state can be significantly influenced by the effect of electron-electron interactions beyond the scope of GGA+U.

We filter the entries of the Materials Project dataset to create our training set. This is because the predictions of our machine learning models can only come from the identification of patterns within this dataset. It is therefore crucial to identify biases and potential obstacles to generalization in this training distribution [29]. An important source of errors comes from the fact that DFT can relax to unstable, high-energy structures. Not only these materials cannot be synthesized and will drive the distribution away from materials of interest, but they will also tend to exhibit atypical features that could confuse training. We thus choose to filter these materials out of the dataset based on their energy above hull computed by DFT. The energy above hull gives the energy of decomposition of a material into a set of stable materials containing all the chemical elements of the original material and whose total formation energy is smaller. We choose heuristically the value of  $E = 0.1\text{eV/atom}$  as a threshold for stability. This results in keeping 68.5% of the materials in the dataset (Fig. 1).

The Materials Project dataset is not specifically focused on magnetic materials and includes non-magnetic (which includes paramagnetic since only spontaneous magnetization is reported), ferromagnetic and antiferromagnetic materials. The number of materials for each magnetic order is indicated in Fig. 2. For our goal of

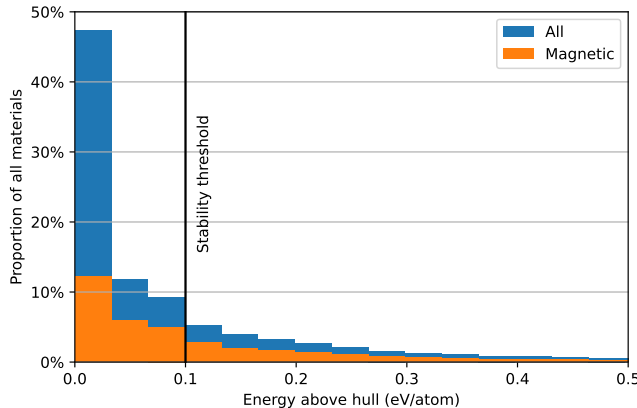


FIG. 1: Distribution of the energy above hull attribute in the Materials Project dataset.

predicting magnetization, having both non-magnetic and magnetic materials is a desirable property: we want the model to identify the factors promoting strong magnetization as well as those inhibiting it. We note that the procedure of filtering out unstable structures helps to alleviate the ferromagnetic bias of DFT. Fig. 1 shows that the proportion of magnetic materials increases with the energy above hull. Fig. 2 further shows that the eliminated materials are more ferromagnetic and ferrimagnetic; the proportion of antiferromagnetic materials slightly increases after filtering.

Fig. 3 shows the distribution of elements in the Materials project dataset, blue indicating the proportion for all materials, and orange the proportion for the subset of magnetic materials. In the latter category, it is not surprising to find transition metals. Oxygen is often present in magnetic materials probably because of the prevalence of perovskite structures that make up 93% of the lower earth mantle's mass. Surprisingly, Li is also often present in magnetic materials, which may this time reflect the interest of researchers in materials containing Li because of the technological importance of batteries.

## 2. ICSD

Having trained models on the Materials Project, our main objective is to identify high magnetization candidates that can readily be synthesized. We use data from the Inorganic Crystal Structures Database (ICSD) to perform this task. It is currently the largest database of experimentally identified crystalline materials.

ICSD data is obtained directly from scientific publications. It includes chemical composition as well as crystal structure data for all of its entries.

Unlike the Materials Project, ICSD includes non-stoichiometric materials. Since our training distribution did not include such materials, we expect that our models will have difficulty generalizing to these materials and

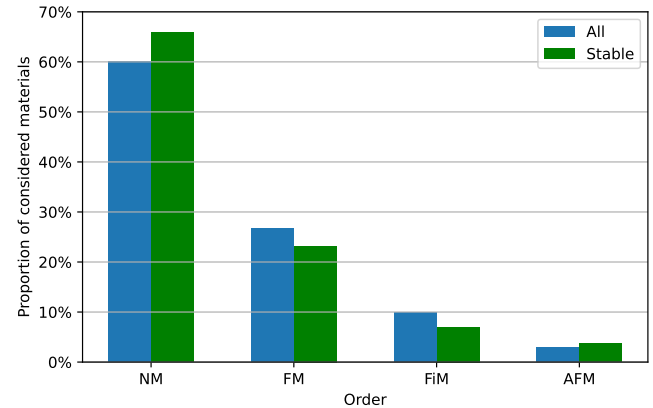


FIG. 2: Distribution of magnetic orders in the Materials Project dataset. NM stands for non-magnetic, FM for ferromagnetic, FiM for ferrimagnetic and AFM for antiferromagnetic.

we have thus removed these entries from the inference dataset. In addition, it is crucial to take into account that the Materials Project and ICSD datasets are not independent. As explained above, the crystal structures of the entries in Materials project are computed starting from ICSD entries. Though some of the structures change significantly through the relaxation process, many of them remain sufficiently similar to the ICSD starting point to be considered as common entries between the two datasets. We have identified the common entries in both datasets and found that out of the 149 798 stoichiometric entries in ICSD, 26 037 have had their properties computed in Materials Project. That leaves 123 761 materials use during inference of magnetization.

The intersection between ICSD and Materials Project also allows us to confirm that filtering based on the values of the energy above hull is appropriate. Looking at the materials in ICSD for which the energy above hull is available from Materials Project, we see on Fig. 4 that the distribution is highly skewed towards values smaller than our threshold of 0.1 eV/atom.

## B. Training and inference setup

Once trained, machine learning algorithms have the important advantage of producing predictions orders of magnitude faster than simulation methods like DFT. We can thus use them to efficiently screen candidate materials in a large database.

We first train a model for each method on the Materials Project dataset. Training is performed by minimizing the mean squared error (MSE) of the predicted magnetization per atom with the Materials Project target. We also report the mean absolute error (MAE) between predicted magnetization and ground-truth values. The Materials Project dataset is split into a training set

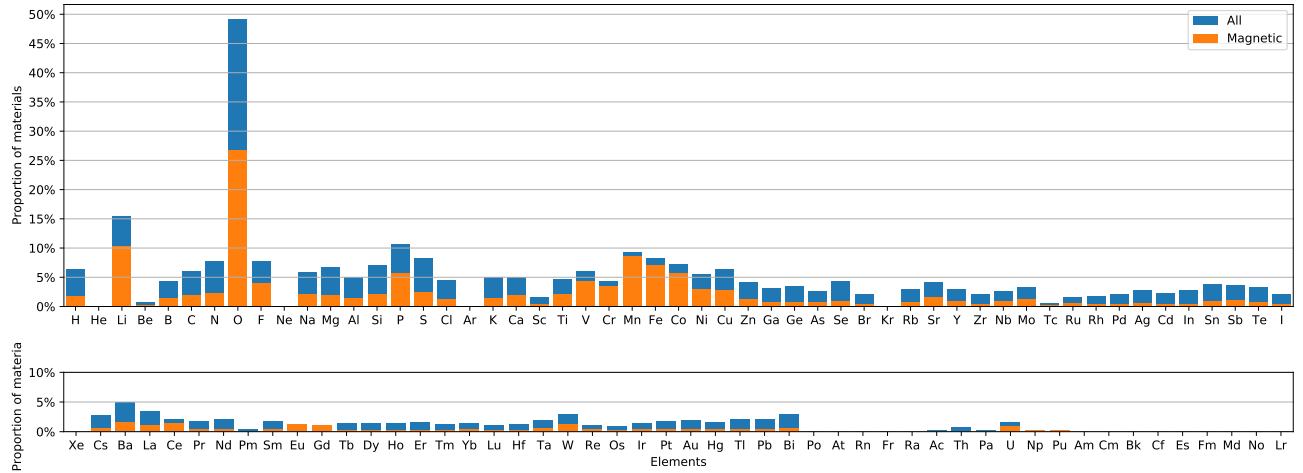


FIG. 3: Histogram of entries in the Materials Project dataset categorized by presence (irrespective of stoichiometry) of a chemical specie. Blue denotes the distribution over all materials and orange over the subset of magnetic materials.

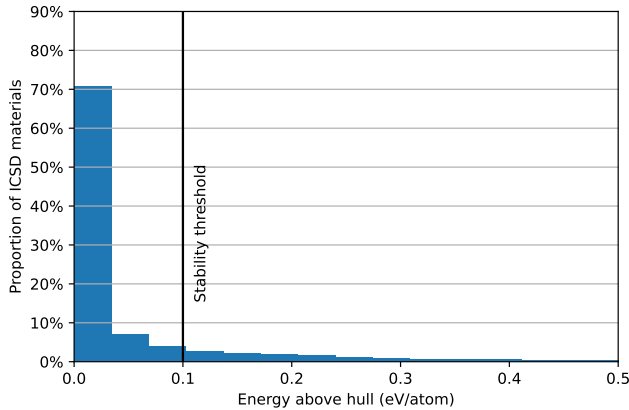


FIG. 4: Distribution of the energy above hull per atom attribute in the Materials Project dataset for the subset of entries that are also in the ICSD dataset.

comprising 80% of the data, a validation set of 10% and a test set of 10%. We compare the performance on the test for each method in Table II. We also train models to predict the formation energy given in Materials Project. Since results on this task are obtained in the original implementations of CGCNN and MEGNet, this allows us to verify that our implementations of the models perform as well as expected.

Inference is performed using the trained model on the ICSD database. As explained above, non-stoichiometric materials are eliminated since they are absent from the training set. In addition, a small fraction of the entries had incomplete crystal structure information and had to be discarded when using GNNs.

### C. Evaluation of methods

We are interested in evaluating the performance of our machine learning models. Aside from random forests and GNNs, we also consider a simple linear model [30]. The linear model is trained using the same descriptor space as the random forest. Since the linear model assumes a simple relation between each descriptor and the target, it is not expected to be accurate. Therefore, it establishes a performance baseline against which more elaborate methods will be compared. We first compare the performance on prediction of the formation energy as this is a popular benchmark for machine learning methods. We find that our models perform on par or slightly better than the original implementations. The difference can be attributed to the fact that we use a different version of the Materials Project dataset as well as different training, validation and test set splits. Our hyperparameters are also slightly different, as detailed in Supplementary Information. We see that neural networks outperform random forests (Table I) by a significant margin.

Then, we evaluate the different models on the magnetic moment prediction task on the Materials Project dataset. Results are shown on Table II. As expected, all models outperform the baseline linear model, although not by a large margin. We find that both neural network architectures perform worst on this task than random forests. This is in strong contrast with the evaluation of prediction accuracy of formation energy. Thus, the common belief that deep models should perform better than models based on handcrafted descriptors is invalidated for this task.

The difference between magnetization and formation energy results may be understood by the fact that random forests could handle imbalance in prediction labels better than neural networks. In our case, the imbalance is

caused by the fact that the distribution of magnetization values is bimodal, with one mode associated with non-magnetic and antiferromagnetic materials and the other with ferromagnetic and ferrimagnetic materials. These modes have significantly different weights in the distribution as shown in Figure 2. It is well known that neural networks are notoriously difficult to train on imbalanced data [31]. In comparison, random forests handle this task better since they can first classify samples according to their magnetic phase and then assign a magnetization value.

Deep models also show a stronger tendency to overfit training data which can explain that they compare worse on MSE than MAE. Neural networks show only a small improvement in MSE with respect to the linear model, which indicates that these models struggle with some materials that are outliers with respect to the training set. By contrast, predictions given by the random forest are more conservative when confronted with materials different from training data.

#### D. Predictions on ICSD

We now apply the trained random forests, CGCNN and MEGNet models on the ICSD dataset. We use the median and standard deviation of the results from the three models to estimate the magnetization and the error. From the previous section, we know that the models have a good performance on the test set of the Materials Project dataset. However, it is not sufficient to determine whether our models perform well on the ICSD dataset or not. To better understand the accuracy of our predictions, we sort the results in decreasing order of the predicted magnetization per kilogram. We remove the entries for which the standard deviation calculated from the random forest, CGCNN and MEGNet results exceeds 35%. Then, we focus on the first 250 materials with the highest predicted magnetic moment per mass unit from this curated list. Through this process, 169 materials are removed because they are duplicates of other entries, which leaves us with 82 unique materials. To gain an insight on the accuracy of our model, we compare the predicted magnetic properties of these 82 materials to available experimental measurements and report our findings in Table III. The list of materials, magnetic orders and associated references used to construct III is available in the Supplementary Information. Notably, we were unable to find experimental reports on the magnetic properties of 22 materials, indicating that our models could indeed be used for the discovery of new magnetic materials. We report our predictions for the magnetic moment of 15 of these materials in Table IV. We note that all of these materials include magnetic rare-earths or magnetic transition metals. It is hence plausible that they are indeed ferromagnets with a large magnetic moment.

With regards to magnetic refrigeration, the rotating magnetocaloric effect is a promising recent research direc-

tion [32–36]. While the traditional magnetocaloric effect is due to the change in magnetization of a material under the successive application and removal of an external magnetic field, the rotating magnetocaloric effect is due to a strong magnetic anisotropy. In such anisotropic materials, the magnetization is locked in a particular crystal direction (the so-called “easy-axis”). In that case, a magnetocaloric effect is seen when the material is rotated in a fixed external magnetic field. Materials that exhibit this rotating magnetocaloric effect must have a strong spin-orbit coupling, which is usually associated to elements with a large atomic number. The materials we show in Table IV that include Eu, Gd and In elements could potentially satisfy this requirement.

Coming back to Table III, we find that 30 materials from the subset of 82 are actually reported as ferromagnetic, or ferrimagnetic with a high magnetic moment per mass unit. The remaining materials, accounting for 37% of our 82 materials sample, are found to be mostly antiferromagnetic. This analysis of a subset of our predictions highlights the challenge in predicting the magnetization from models trained of the Materials Project dataset. The ferromagnetic bias in the training set may explain the discrepancy between the predicted ferromagnetic orders and the actual non-ferromagnetic orders observed experimentally. This emphasizes that the discrepancies between high-throughput DFT calculations and experiments can mean that the high performance of a model trained on a DFT dataset does not necessarily translate to accurate predictions when it is applied to an experimental database.

To further illustrate the issues arising in the prediction of the magnetic moment from DFT calculation, we now focus on five materials that contain gadolinium out of the sample of 85 materials described above. Many Gd-based materials are well-known ferromagnets, and their magnetic properties have been investigated thoroughly, which allows for quantitative comparison to our results. We report the predicted magnetic moment per mass unit as well as the measured magnetic moment and magnetic order of 5 Gd-based materials in Table V. Averages and standard deviations of the predictions of random forests, CGCNN and MEGNet are shown.

The most notable discrepancy between the measured and predicted magnetic moment is that of  $\text{GdH}_2$ : experimental evidence shows that it is antiferromagnetic, while our models predict it as having a high magnetization, comparable to that of known-ferromagnet Gd. Our models also overestimate the magnetization of  $\text{GdB}_2$ , though the comparison might be hindered by the fact that the measurements were done at high temperature (275K). In the case of  $\text{GdMg}$ , the predicted magnetic moments per mass units exceed the measured ones by approximately 100  $\text{J}/(\text{T} \times \text{kg})$ . This discrepancy could be due to the fact that this material, experimentally, has a non-collinear ferromagnetic ground state, whereas our models seem to consider it as a ferromagnet. Finally, our predictions are quite accurate for the two remaining materials,

Gd and GdN. Both of them are reported as ferromagnets from experiments.

### III. DISCUSSION

To identify materials with a large magnetic moment per kilogram, we have trained random forests and two state-of-the-art deep-learning graph convolutional algorithms, CGCNN and MEGNet, on the Materials Project dataset. Magnetic properties in the training set are computed using DFT methods. The three machine-learning methods show comparable accuracy on the test sets. Differences in estimates for the mean average error and mean squared error suggest that the predicted magnetic moment per atom is accurate to better than 0.05 Bohr magneton per atom.

We used the trained algorithms to search for candidate materials with large magnetic moments per kilogram in the ICSD database. That database contains materials that have been synthesized. Table IV lists the most promising materials. These deserve experimental attention, for example in the context of magnetic refrigeration.

### IV. METHODS

The setup is that of a supervised learning task: given a training set of materials with features  $\mathbf{X}$  and known ground-truth targets  $\mathbf{Y}$ , the algorithm is tasked to learn a prediction function  $\mathbf{Y}' = f_{\theta}(\mathbf{X})$ . Training parameters  $\theta$  are optimized to minimize a loss function  $\mathcal{L}(\mathbf{Y}, \mathbf{Y}')$ .

In the following subsections, we describe the learning algorithms we have used. Hyperparameters are given in Supplementary Information. Fig. 5 summarizes schematically the methods that we use.

#### A. Random Forests

The random forest [37] is a tree-based machine learning algorithm that has been widely used for materials property prediction [4–6]. Random forests have yielded encouraging results for similar material design tasks, for example finding superconductors [38, 39]. At the root of any tree-based method lies the decision tree, which carries out consecutive binary splits in the descriptor space of the data (see Figure 5a). Single decision trees, however have the major drawback of frequently overfitting the training data. Random forests go around this problem by averaging the predictions of multiple decision trees. Each tree is built differently to ensure that there is some variance in the generated forest. Randomness is implemented by choosing a subset of the descriptors to be available to the usual tree algorithm every time the algorithm makes a split. The subset is different for every split. The number of descriptors in the subset is a hyperparameter called

“Available features per split”. The use of random forests is motivated in our case by their relative simplicity and efficiency [40]. We use Scikit-learn’s [30] implementation of the random forest methods.

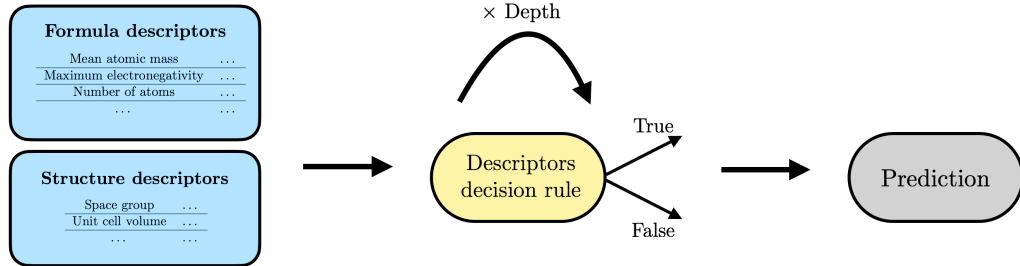
The model takes descriptors handcrafted for each sample material as input. The algorithm achieves much better performance if descriptors are well adapted to the task. The properties found in both Materials Project and ICSD, such as density and crystal structure, can be employed in our case. Inspired by other works [38, 39], most of the descriptors have been built from the chemical formula of the materials: starting from atomic properties, such as the ground-state magnetic moment, the electronegativity, the atomic mass or the ground state d-shell electrons, we compute the mean value, the maximum value or the standard deviation of each of these properties to form descriptors. We design more than 400 descriptors in this way for each material encountered.

Using this large descriptor space would lead to overfitting. In addition to yielding better predictions, identifying the best set of descriptors comes with the added benefit of giving more interpretability to the model. Because of the large number of descriptors and material entries, forward and backward descriptor selection methods one would typically use for this task require an unreasonable amount of computational resources and time. We therefore design a descriptor selection scheme, which mixes both forward and backward descriptor selection in order to efficiently find which descriptors are relevant for the task (details in Supplementary Information).

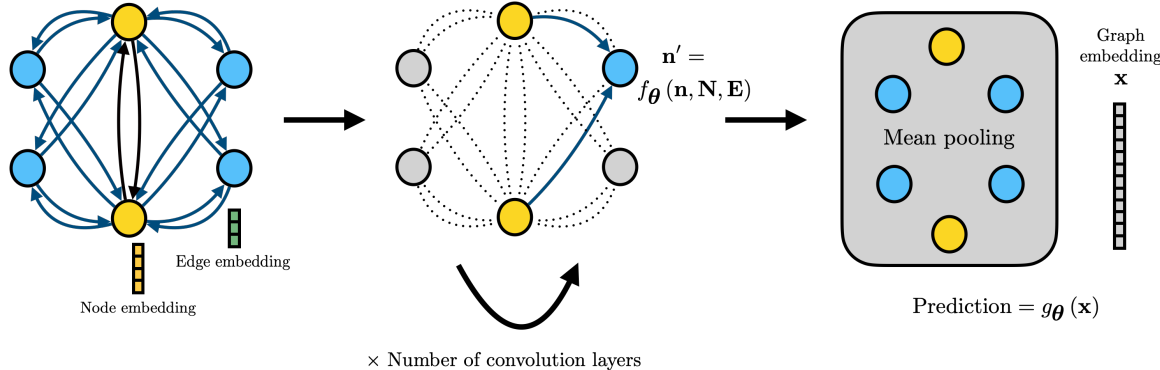
#### B. Graph Neural Networks

Graph neural networks (GNNs) are deep learning architectures that are widely used for molecular-property prediction and generation [41, 42]. Their use in the context of materials is however recent. The main advantage of using GNNs for materials property prediction compared to other machine learning methods is that they only take as input a graph encoding of the material that naturally encodes structure information. The need for using handcrafted features is eliminated, as the deep models acts as a *feature extractor*. This ability to learn a representation adapted to the task at hand from the raw data has been key to the success of deep learning in a variety of domains. However, it is essential to note that this additional expressivity (the complexity and diversity of prediction functions that can be learned) comes at the cost of interpretability. It is notoriously difficult to know how a neural network selects specific features for predictions [43]. For this reason, we deem more appropriate to use neural networks in conjunction with random forests, a method that allows explicit descriptor construction and selection.

Here we use two architectures, CGCNN [12] and MEGNet [13] that have been chosen for their performance on other properties of the Materials Project dataset as well



(a) Illustration of a decision tree. First, descriptors are computed from the chemical formula and the structural properties. A series of decisions are then taken using the descriptors. After a number of decisions, the final prediction is made.



(b) Illustration of a GNN. A graph is built from the crystal unit cell. Each atom is mapped to a node and an edge is drawn between two nodes if they share a Voronoi face. Both nodes and edges have associated embedding vectors. The graph then goes through a series of graph convolution operations parametrized by the neural network  $f_\theta$ . Finally, the features of all the nodes are averaged and the resulting vector goes through a multilayer perceptron  $g_\theta$  that outputs the prediction.

FIG. 5: Methods used for property prediction.

as their good training speed. For each material, the crystal unit cell is mapped to a sparse graph. This is done by associating each atom to a node and linking two nodes if they share a Voronoi face and are within a cutoff distance of 13 angstroms. Edges are also added if a face is shared with an atom outside the unit cell to enforce periodic boundary conditions. In this case, the edge is with respect to the corresponding atom in the unit cell. Around 5% of structures resulted in disconnected graphs and were discarded. Descriptors based on the chemical formula are here replaced by one-hot encodings of graph nodes based on the atomic species. This allows to capture all the information on atoms composing the unit cell. An encoding based on the distance for edges is used as well. Taking inspiration from Schnet [14], this distance is expanded on a Gaussian basis of functions, with details specified in Supplementary Information.

Each architecture takes these labeled graphs as input and applies successive graph convolution layers to them (see Figure 5b). The main difference between the two models revolves around the design of these layers, which is detailed in the original papers. After a number of passes in convolution layers, node and edge representations are pooled and sent to a regressor multilayer perceptron that outputs the final prediction. For each architecture, we use the original hyperparameters with a few modifications detailed in Supplementary Informa-

tion. Training is performed using stochastic gradient descent with the Adam optimizer [44] as well as a learning rate scheduler.

## DATA AVAILABILITY

Data from the Materials Project dataset is freely available using their API. Documentation for this API is available at <https://docs.materialsproject.org/open-apis/the-materials-api/>. ICSD is under a proprietary license.

## CODE AVAILABILITY

The code used to obtain our results is available from the corresponding author upon reasonable request.

## ACKNOWLEDGMENTS

We are grateful to Hong Guo and Peter Kang for early access to iMat and to Patrick Fournier, Shengrui Wang, Yoshua Bengio, Simon Blackburn and Michel Côté for useful discussions.

This work was supported in part by the Canada First Research Excellence Fund (Institut quantique IQ3-2019 (C.G.-N.) and IVADO (S.-O.K. and S.V.)), by the Natural Sciences and Engineering Research Council of Canada (NSERC) under grant RGPIN-2019-05312 (A.-M.S.T.), by a Vanier scholarship from NSERC (C.G.-N.), and by a USRA scholarship from NSERC (B.G.-P.). Calculations were performed on computers provided by the Canadian Foundation for Innovation, the Ministère de l'Éducation des Loisirs et du Sport (Québec), Calcul Québec, and Compute Canada.

## AUTHOR CONTRIBUTIONS

All authors contributed to designing the study and analyzing results. S.-O.K. wrote the code for the deep learning models. B.G.-P. and M.-A. G. wrote the code for random forests models. S.-O.K. and S.V. analyzed the datasets. S.-O.K., B.G.-P, M.-A.G., A.-M.S.T. and C. G.-N. wrote the paper. A.-M.S.T, S.V. and C.G.-N. provided supervision for the project.

## COMPETING INTERESTS

The authors declare no competing interests.

Model	MAE ( $\mu_B/\text{atom}$ )	MSE ( $\mu_B/\text{atom}$ )
CGCNN (Original)	0.039	-
MEG-Net (Original)	0.028	-
Linear Model	0.302	0.169
Random Forest	0.100	0.038
CGCNN (Ours)	0.023	0.003
MEG-Net (Ours)	0.031	0.004

TABLE I: Performance on the test set of the various models on prediction of the formation energy per atom using the Materials Project dataset.

Model	MAE ( $\mu_B/\text{atom}$ )	MSE ( $\mu_B/\text{atom}$ )
Linear	0.100	0.030
Random Forest	0.042	0.016
CGCNN	0.052	0.026
MEG-Net	0.052	0.026

TABLE II: Performance on the test set of the various models on prediction of the magnetic moment per atom using the Materials Project dataset.

Magnetic order reported from experiments	Number of materials in the reduced list
Ferromagnetic/Ferrimagnetic	30 (37%)
Antiferromagnetic	21 (26%)
Non-magnetic/paramagnetic	4 (4%)
Other	5 (6%)
Order not reported	22 (27%)

TABLE III: We find the 85 experimentally characterized materials with the highest predicted magnetization from our predictions on ICSD. Table shows the distribution of experimentally observed magnetic orders for these materials.

Chemical formula	Lattice symmetry	Moment per mass (J/(T × kg))	Rare earths
EuAlH <sub>5</sub>	Orthorhombic	550 ±170	Yes
EuMg <sub>2</sub>	Trigonal	500 ±20	Yes
(FeH <sub>6</sub> )H <sub>2</sub>			
Fe <sub>23</sub> Y <sub>6</sub> H <sub>22</sub>	Cubic	220 ±60	Yes
Mg <sub>3</sub> MnH <sub>6</sub>	Monoclinic	240 ±70	No
Gd <sub>6</sub> Mn <sub>23</sub> H <sub>24</sub>	Cubic	230 ±30	Yes
Eu <sub>2</sub> H <sub>3</sub> Cl	Trigonal	220 ±20	Yes
MgEu	Cubic	220 ±1	Yes
Eu <sub>2</sub> FeH <sub>6</sub>	Cubic	220 ±20	Yes
GdAl	Cubic	220 ±3	Yes
Gd <sub>2</sub> CF <sub>2</sub>	Trigonal	210 ±10	Yes
MgMn <sub>4</sub> O <sub>8</sub>	Triclinic	200 ±60	No
Eu <sub>3</sub> OIn	Cubic	200 ±30	Yes
Eu <sub>2</sub> H <sub>3</sub> Br	Trigonal	200 ±20	Yes
InGd <sub>3</sub> C	Cubic	200 ±2	Yes
Fe <sub>3</sub> Ni	Cubic	200 ±100	No

TABLE IV: Predictions of the largest magnetic moments per mass on the ICSD database. Averages and standard deviations of the predictions of random forests, CGCNN and MEGNet are shown.

Chemical formula	Median predicted moment per mass	Measured moment per mass	Magnetic order from experiment
GdH <sub>2</sub>	249 ± 2	-	AFM [45]
Gd	230 ± 20	273	FM [46]
GdN	234 ± 5	228	FM [47]
GdMg	233 ± 0.4	138	FM (non-collinear) [48]
GdB <sub>2</sub>	222 ± 5	19.5 (at 275K)	FM [49]

TABLE V: Predictions of magnetic moment per mass on the ICSD database for materials that contain gadolinium. Averages and standard deviations of the predictions of random forests, CGCNN and MEGNet are shown. The experimentally measured magnetic moment per mass is also given for comparison (when available). All magnetic moments are listed in J/(T × kg).

---

[1] Z.-L. Liu, P. Kang, Y. Zhu, L. Liu, and H. Guo, Material informatics for layered high-*tc* superconductors, *APL Materials* **8**, 061104 (2020).

[2] Y. Wu, J. Guo, R. Sun, and J. Min, Machine learning for accelerating the discovery of high-performance donor/acceptor pairs in non-fullerene organic solar cells, *npj Computational Materials* **6**, 120 (2020).

[3] C. Ortiz, O. Eriksson, and M. Klintenberg, Data mining and accelerated electronic structure theory as a tool in the search for new functional materials, *Computational Materials Science* **44**, 1042 (2009).

[4] L. Ward, A. Agrawal, A. Choudhary, and C. Wolverton, A general-purpose machine learning framework for predicting properties of inorganic materials, *npj Computational Materials* **2**, 10.1038/npjcompumats.2016.28 (2016).

[5] G. A. Landrum and H. Genin, Application of machine-learning methods to solid-state chemistry: ferromagnetism in transition metal alloys, *Journal of Solid State Chemistry* **176**, 587 (2003), special issue on The Impact of Theoretical Methods on Solid-State Chemistry.

[6] T. D. Rhone, W. Chen, S. Desai, S. B. Torrisi, D. T. Larson, A. Yacoby, and E. Kaxiras, Data-driven studies of magnetic two-dimensional materials, *Scientific Reports* **10**, 10.1038/s41598-020-72811-z (2020).

[7] J. J. Möller, W. Körner, G. Krugel, D. F. Urban, and C. Elsässer, Compositional optimization of hard-magnetic phases with machine-learning models, *Acta Materialia* **153**, 53 (2018).

[8] A. Jain, S. P. Ong, G. Hautier, W. Chen, W. D. Richards, S. Dacek, S. Cholia, D. Gunter, D. Skinner, G. Ceder, and K. a. Persson, The Materials Project: A materials genome approach to accelerating materials innovation, *APL Materials* **1**, 011002 (2013).

[9] S. Kirklin, J. E. Saal, B. Meredig, A. Thompson, J. W. Doak, M. Aykol, S. Rühl, and C. Wolverton, The open quantum materials database (oqmd): assessing the accuracy of dft formation energies, *npj Computational Materials* **1**, 15010 (2015).

[10] C. J. Court and J. M. Cole, Magnetic and superconducting phase diagrams and transition temperatures predicted using text mining and machine learning, *npj Computational Materials* **6**, 10.1038/s41524-020-0287-8 (2020).

[11] S. Curtarolo, W. Setyawan, G. L. Hart, M. Jahnatek, R. V. Chepulskii, R. H. Taylor, S. Wang, J. Xue, K. Yang, O. Levy, M. J. Mehl, H. T. Stokes, D. O. Demchenko, and D. Morgan, Aflow: An automatic framework for high-throughput materials discovery, *Computational Materials Science* **58**, 218 (2012).

[12] T. Xie and J. C. Grossman, Crystal graph convolutional neural networks for an accurate and interpretable prediction of material properties, *Physical Review Letters* **120**, 10.1103/physrevlett.120.145301 (2018).

[13] C. Chen, W. Ye, Y. Zuo, C. Zheng, and S. P. Ong, Graph networks as a universal machine learning framework for molecules and crystals, *Chemistry of Materials* **31**, 3564 (2019), <https://doi.org/10.1021/acs.chemmater.9b01294>.

[14] K. Schütt, P.-J. Kindermans, H. E. S. Felix, S. Chmiela, A. Tkatchenko, and K.-R. Müller, Schnet: A continuous-filter convolutional neural network for modeling quantum interactions, in *Advances in Neural Information Processing Systems* (2017) pp. 991–1001.

[15] H. Nakamura, The current and future status of rare earth permanent magnets, *Scripta Materialia* **154**, 273 (2018).

[16] Weiss, Pierre and Piccard, Auguste, Le phénomène magnétocalorique, *J. Phys. Theor. Appl.* **7**, 103 (1917).

[17] J. R. Gómez, R. F. Garcia, A. D. M. Catoira, and M. R. Gómez, Magnetocaloric effect: A review of the thermodynamic cycles in magnetic refrigeration, *Renewable and Sustainable Energy Reviews* **17**, 74 (2013).

[18] A. Smith, C. R. Bahl, R. Bjørk, K. Engelbrecht, K. K. Nielsen, and N. Pryds, Materials challenges for high performance magnetocaloric refrigeration devices, *Advanced Energy Materials* **2**, 1288 (2012).

[19] G. V. Brown, Magnetic heat pumping near room temperature, *Journal of Applied Physics* **47**, 3673 (1976), <https://doi.org/10.1063/1.323176>.

[20] V. K. Pecharsky and K. A. Gschneidner, Jr., Giant magnetocaloric effect in  $Gd_5(Si_2Ge_2)$ , *Phys. Rev. Lett.* **78**, 4494 (1997).

[21] L. Breiman, Random forests, *Machine learning* **45**, 5 (2001).

[22] G. James, D. Witten, T. Hastie, and R. Tibshirani, *An Introduction to Statistical Learning*, 8th ed. (Springer, New York, 2017).

[23] A. Liaw, M. Wiener, *et al.*, Classification and regression by randomforest, *R news* **2**, 18 (2002).

[24] G. Bergerhoff and I. Brown, Crystallographic databases (International Union of Crystallography, Chester, 1987).

[25] G. Kresse and J. Furthmüller, Efficient iterative schemes for ab initio total-energy calculations using a plane-wave basis set, *Phys. Rev. B* **54**, 11169 (1996).

[26] K. Lejaeghere, V. V. Speybroeck, G. V. Oost, and S. Cottenier, Error estimates for solid-state density-functional theory predictions: An overview by means of the ground-state elemental crystals, *Critical Reviews in Solid State and Materials Sciences* **39**, 1 (2014).

[27] M. K. Horton, J. H. Montoya, M. Liu, and K. A. Persson, High-throughput prediction of the ground-state collinear magnetic order of inorganic materials using density functional theory, *npj Computational Materials* **5**, 64 (2019).

[28] E. Pavarini, Solving the strong-correlation problem in materials, *La Rivista del Nuovo Cimento* **10**.10007/s40766-021-00025-8 (2021).

[29] V. Gudivada, A. Apon, and J. Ding, Data quality considerations for big data and machine learning: Going beyond data cleaning and transformations, *International Journal on Advances in Software* **10**, 1 (2017).

[30] F. Pedregosa, G. Varoquaux, A. Gramfort, V. Michel, B. Thirion, O. Grisel, M. Blondel, P. Prettenhofer, R. Weiss, V. Dubourg, J. Vanderplas, A. Passos, D. Cournapeau, M. Brucher, M. Perrot, and Édouard Duchesnay, Scikit-learn: Machine learning in python, *Journal of Machine Learning Research* **12**, 2825 (2011).

[31] J. M. Johnson and T. M. Khoshgoftaar, Survey on deep learning with class imbalance, *Journal of Big Data* **6**, 1 (2019).

[32] M. Balli, S. Mansouri, D. Z. Dimitrov, P. Fournier, S. Jandl, and J.-Y. Juang, Strong conventional and rotating magnetocaloric effects in  $TbVO_4$  crystals over a wide cryogenic temperature range, *Phys. Rev. Materials* **4**, 114411 (2020).

[33] M. Balli, S. Jandl, P. Fournier, and M. M. Gospodinov, Anisotropy-enhanced giant reversible rotating magnetocaloric effect in homn2o5 single crystals, *Applied Physics Letters* **104**, 232402 (2014).

[34] M. Balli, S. Jandl, P. Fournier, and D. Z. Dimitrov, Giant rotating magnetocaloric effect at low magnetic fields in multiferroic tbmn2o5 single crystals, *Applied Physics Letters* **108**, 102401 (2016), <https://doi.org/10.1063/1.4943109>.

[35] M. Orendáć, S. Gabáni, E. Gazo, G. Pristás, N. Shitsevalova, K. Siemensmeyer, and K. Flachbart, Rotating magnetocaloric effect and unusual magnetic features in metallic strongly anisotropic geometrically frustrated tmb4, *Scientific Reports* **8**, 10933 (2018).

[36] H. Zhang, Y. Li, E. Liu, Y. Ke, J. Jin, Y. Long, and B. Shen, Giant rotating magnetocaloric effect induced by highly texturing in polycrystalline dynisi compound, *Scientific Reports* **5**, 11929 (2015).

[37] Tin Kam Ho, Random decision forests, in *Proceedings of 3rd International Conference on Document Analysis and Recognition*, Vol. 1 (1995) pp. 278–282 vol.1.

[38] V. Stanev, C. Oses, A. G. Kusne, E. Rodriguez, and J. Paglione, Machine learning modeling of superconducting critical temperature, *npj Computational Materials* **4** (2018).

[39] Z.-L. Liu, P. Kang, Y. Zhu, L. Liu, and H. Guo, Material informatics for superconductors (2019).

[40] G. Louppe, *Understanding Random Forests: From Theory to Practice*, Ph.D. thesis, University of Liège (2015).

[41] D. K. Duvenaud, D. Maclaurin, J. Iparraguirre, R. Bombarell, T. Hirzel, A. Aspuru-Guzik, and R. P. Adams, Convolutional networks on graphs for learning molecular fingerprints, in *Advances in neural information processing systems* (2015) pp. 2224–2232.

[42] J. Gilmer, S. S. Schoenholz, P. F. Riley, O. Vinyals, and G. E. Dahl, Neural message passing for quantum chemistry, in *Proceedings of the 34th International Conference on Machine Learning*, Proceedings of Machine Learning Research, Vol. 70, edited by D. Precup and Y. W. Teh (PMLR, International Convention Centre, Sydney, Australia, 2017) pp. 1263–1272.

[43] S. Chakraborty, R. Tomsett, R. Raghavendra, D. Harborne, M. Alzantot, F. Cerutti, M. Srivastava, A. Preece, S. Julier, R. M. Rao, *et al.*, Interpretability of deep learning models: A survey of results, in *2017 IEEE smartworld, ubiquitous intelligence & computing, advanced & trusted computing, scalable computing & communications, cloud & big data computing, Internet of people and smart city innovation (smartworld/SCALCOM/UIC/ATC/CBDcom/IOP/SCI)* (IEEE, 2017) pp. 1–6.

[44] D. P. Kingma and J. Ba, Adam: A method for stochastic optimization, *arXiv preprint arXiv:1412.6980* (2014).

[45] S. Hémon, R. A. Cowley, R. C. C. Ward, M. R. Wells, L. Douyset, and H. Ronnow, Magnetic structure of gd, GdH2and NdH2single crystal films, *Journal of Physics: Condensed Matter* **12**, 5011 (2000).

[46] J. H. Queen, *Saturation moments of Gd alloys*, Ph.D. thesis, Iowa State University (1981).

[47] R. A. Cutler and A. W. Lawson, Synthesis and magnetic behavior of gdn, *Journal of Applied Physics* **46**, 2739 (1975).

[48] R. Aleonard, P. Morin, J. Pierre, and D. Schmitt, Magnetic properties, magnetic structure of gdmg and tbmg compounds, *Solid State Communications* **17**, 599 (1975).

[49] H. Gencer, T. Izgi, V. S. Kolat, and S. Atalay, Magnetic and magnetocaloric properties of gdb2 compound, *Optoelectronics and Advanced Materials - Rapid Communications* **6**, 875 (2012).

# Prediction of Large Magnetic Moment Materials With Graph Neural Networks and Random Forests

## Supplementary Information

Sékou-Oumar Kaba,<sup>1, 2,\*</sup> Benjamin Groleau-Paré,<sup>3</sup> Marc-Antoine Gauthier,<sup>3</sup> André-Marie Tremblay,<sup>3</sup> Simon Verret,<sup>1, 3</sup> and Chloé Gauvin-Ndiaye<sup>3</sup>

<sup>1</sup>*Mila - Quebec Artificial Intelligence Institute & IVADO - Institut de Valorisation des Données, Montréal, Québec, Canada H2S 3H1*

<sup>2</sup>*School of Computer Science, McGill University, Montréal, Québec, Canada H3A 0E9*

<sup>3</sup>*Département de physique & Institut Quantique, Université de Sherbrooke, Québec, Canada J1K 2R1*

(Dated: November 30, 2021)

### I. HYPERPARAMETERS

For random forests, tuning each hyperparameter individually and in sequence prevents one from detecting possible relations between parameters. Therefore, the ultimate set of hyperparameters was found using random search.

For neural network methods, we used the same hyperparameters for CGCNN and MEGNet for convenience reasons as well as to avoid excessive hyperparameter tuning. General hyperparameters were optimized through grid search. Other values were selected in accordance with the original architectures or by convenience given the available hardware.

Hyperparameter	Value
Number of descriptors	98
Bootstrap	None
Available features per split	32.5%
Minimum samples for a split	4
Minimum samples per leaf	2
Minimum depth	None

(a) Random forest models

	Hyperparameter	Value
General	Starting learning rate	0.001
	Patience	25
	Learning rate factor	0.5
	Batch size	1024
CGCNN	Site embedding size	100
	Bond embedding size	20
	Bond Gaussian basis size	10
	Maximum bond distance	5.2
	Hidden layer size	100
	Number of convolution layers	2
	Number of output layers	3
MEGNET	Site embedding size	36
	State embedding size	36
	Bond embedding size	36
	Bond Gaussian basis size	100
	Maximum bond distance	5.2
	Number of Megnet layers	3
	Megnet layer hidden size	64
	Number of output layers	3
	Output layer 1 hidden size	32
	Output layer 2 hidden size	16

(b) Graph neural network models

TABLE I: Hyperparameter values.

\* kabaseko@mila.quebec

## II. FEATURE SELECTION

Our feature selection method converges iteratively towards the final set of descriptors. The scheme works by chunking the training data and descriptor space into smaller sets on which forward and backward feature selection methods are then performed.

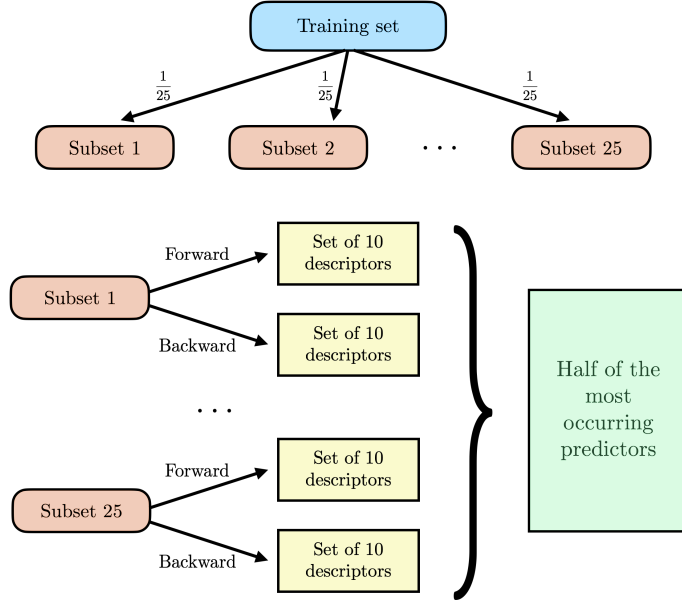


FIG. 1: Schematic view of one step of the feature selection scheme.

We describe the feature selection method, and give a schematic view of this process in Fig. 1. Suppose one wants to build a random forest regressor from a 100,000-entries training set using only a handful of features from a very large descriptor space. Performing a regular forward or backward feature selection on the whole training set to obtain an optimal set of descriptors would require an unreasonable amount of computational resources and time. To reduce the computational time, one splits its training dataset in 25 equal parts, which results in chunks of data of 4000 materials each. One then performs a forward and a backward feature selection on every chunk of data for a total of 50 calculations. Since the dataset size is much smaller, the computation time is significantly reduced. One then counts the occurrence of each descriptor in the final set of 10 features of the 50 calculations and removes half of the descriptors based on their low or null occurrence. The same operation can be repeated on the new descriptor space to remove even more features and get closer to an optimal final set of descriptors. However, this time, the dataset can be split in fewer chunks since the are less descriptors to choose from. Note that the choices made in this example, such as the number of chunks and the number of descriptors removed at each step, are arbitrary and chosen for convenience.

### III. DESCRIPTOR IMPORTANCE

We use the descriptor importance score [1] available in Scikit-learn. The method works by computing how on average each descriptor decreases the impurity when used in a split. The mean impurity decrease is computed for all descriptors and normalized over the entire descriptor set to give the importance score displayed in Table II. Some descriptors are built using three different lists of atoms that we call L1, L2 and L3, which are defined below Table II.

From Table II, we see that most descriptors have an almost equal and very small importance. Let us focus on the first four descriptors. We first note that these four descriptors are all directly linked to the atomic magnetic properties of the elements in a chemical formula. Hence, it is not so surprising that they are especially relevant for predicting the magnetic moment of a material.

The two descriptors with the highest importance are calculated from weighted averages over the L3 list. The descriptor with the highest importance (22.739%), “weighted average of f-shell valence electrons (L3)” gives a weight of 1 for each atom in the unit cell that contains valence electrons that are in the f-shell and that are also in the list L3 and a weight 0 otherwise. The list L3 contains atoms that generally have large atomic moments. Since this descriptor selects atoms with an f-shell in the valence band, rare-earths are selected, and it is not surprising that this descriptor provides splits that sort out the data the most. It is by far the most important descriptor.

The next three descriptors with the highest importance are all calculated from the atomic magnetic moment. More specifically, the descriptor “weighted avg. (L3) at. magnetic moment”, with an importance of 9.177%, calculates the weighted average of the actual atomic magnetic moments for elements that appear in the chemical formula and in the L3 list. In addition to elements with unfilled f-shell, that list contains elements that have unfilled 3d-shell electrons but no electrons in the f-shell. The magnetic moments of the transition metals with electrons in the 3d-shell are generally smaller than the magnetic moments of atoms having unfilled f-shell, which increases the MSA and the MAE, leading to a smaller importance, as defined above, of this criterion. Nevertheless, having magnetic atoms in its chemical formula clearly makes a compound likely to be magnetic so this criterion is the second most important.

The other two descriptors that have an importance above 5% are “Max. among mag. at. magnetic moment” and “Max. at. magnetic moment”, with importance of 7.629% and 7.424% respectively. It turns out that, due to the way we construct the descriptors, both of these descriptors calculate the same quantity, which explains why they have the same importance. These descriptors give the highest value of the atomic magnetic moment out of all the elements in a given chemical formula. In the case where there is an atom in the chemical formula with a magnetic moment that dominates that of other atoms, it is quite unlikely that this magnetic moment will be hidden in an antiferromagnetic state of the material for example. A ferromagnetic state becomes more likely.

The first 16 descriptor account for nearly 75% of the total importance score. However, the remaining 82 descriptors still play an important role in the decision trees. These descriptors allow finer cuts in the data which are crucial to the algorithm performance. To test the relevance of these least important descriptors, we ran the random forest algorithm using only the 16 most important descriptors according to Table II, yielding an MAE of 0.072 and an MSE of 0.029, both substantially larger than when the 98 descriptors are used (MAE of 0.042 and MSE of 0.016).

Feature	Importance (%)	Feature	Importance (%)
Weighted avg. (L3) f shell valence el.	22.739	Avg. at. density	0.357
Weighted avg. (L3) at. magnetic moment	9.177	Weighted avg. (L1) at. column	0.351
Max. among mag. at. magnetic moment	7.629	Avg. at. valence el. (Magpie)	0.335
Max. at. magnetic moment	7.424	Min. among mag. at. valence el. (Magpie)	0.328
Weighted avg. (L3) at. valence el. (iMat)	4.424	Weighted avg. (L1) number of	0.32
Weighted avg. (L3) at. d+f shells unfilled el.	3.238	Std. at. valence el. (wikipedia)	0.317
Avg. among mag. (L2) at. magnetic moment	2.875	Std. at. covalent radius	0.31
Min. among mag. at. electron affinity	2.132	Min. among mag. Z	0.268
Weighted avg. (L3) at. volume	2.081	Std. number of	0.264
Weighted avg. (L3) at. volume mendel	2.013	Avg. at. valence el. (wikipedia)	0.252
Weighted avg. (L3) at. polarizability	1.912	Avg. among mag. (L2) at. valence el. (iMat)	0.244
Avg. among mag. (L2) at. electron affinity	1.846	Avg. number of	0.225
Avg. among mag. (L2) at. boiling T	1.752	Avg. at. p shell valence el.	0.215
Weighted avg. (L3) at. valence el. (wikipedia)	1.58	Max. among mag. at. volume	0.214
Weighted avg. (L3) at. unfilled el.	1.562	Avg. among mag. (L2) at. density	0.199
Weighted avg. (L3) f shell unfilled el.	1.234	Max. at. volume	0.196
Weighted avg. (L3) number of	0.977	Min. among mag. at. mass	0.186
Weighted avg. (L2) f shell valence el.	0.924	Min. el. binding energy	0.162
Weighted avg. (L3) at. mass	0.866	Min. at. cohesive energy	0.154
Std. at. electron affinity	0.862	Max. at. polarizability	0.145
Max. at. cohesive energy	0.76	Max. at. column	0.145
Weighted avg. (L3) at. valence el. (Magpie)	0.745	Avg. among mag. (L2) at. column	0.124
Nb. sites	0.705	Max. number of	0.124
Mag. avg. bond length (L3)	0.697	Max. difference number of	0.124
Mag. avg. bond length (L2)	0.67	Max. among mag. at. melting T	0.122
Max. difference at. volume	0.655	Max. at. melting T	0.121
Avg. among mag. (L2) at. volume	0.649	Max. difference at. p shell valence el.	0.121
Avg. at. cohesive energy	0.606	Min. at. boiling T	0.117
Std. among mag. f shell unfilled el.	0.603	Max. difference d shell unfilled el.	0.112
Mag. avg. bond length (L1)	0.584	Min. at. electronegativity	0.111
Std. at. p shell valence el.	0.563	Min. among mag. el. binding energy	0.11
Mag. std. bond angle (L3)	0.561	Max. among mag. number of	0.108
Weighted avg. (L3) at. electron affinity	0.553	Max. d shell valence el.	0.103
Weighted avg. (L2) at. magnetic moment	0.536	Max. at. valence el. (wikipedia)	0.096
Max. among mag. at. boiling T	0.485	Min. among mag. first ionization energy	0.095
Avg. at. volume	0.464	Max. at. p shell valence el.	0.088
Avg. at. electron affinity	0.451	Avg. among mag. (L2) at. row	0.081
Mag. std. bond length (L3)	0.451	Max. at. unfilled el. number	0.078
Avg. among mag. (L2) at. electronegativity	0.438	Max. among mag. mendeleev number	0.073
Weighted avg. (L3) at. column	0.436	Max. among mag. d shell valence el.	0.072
Mag. std. bond angle (L2)	0.436	Max. at. valence el. (iMat)	0.061
Weighted avg. (L2) number of	0.434	Min. among mag. mendeleev number	0.049
Mag. std. bond length (L2)	0.425	Min. among mag. at. electronegativity	0.045
Mag. std. bond length (L1)	0.416	Max. among mag. at. d+f shells unfilled el.	0.042
Weighted avg. (L3) mendeleev number	0.402	Max. at. d+f shells unfilled el.	0.038
Avg. f shell unfilled el.	0.397	Avg. among mag. (L2) f shell unfilled el.	0.03
Avg. at. unfilled el.	0.392	Max. among mag. f shell unfilled el.	0.025
Avg. at. boiling T	0.376	Max. f shell valence el.	0.024
Avg. at. melting T	0.365	Max. f shell unfilled el.	0.019

TABLE II: List of descriptors ordered by importance score. The “valence electrons” atomic property differed from one source to another (iMat[2], Magpie[3] and Wikipedia[4]). Therefore, the source of the descriptors based on this property is specified in parenthesis.

Below are the three subsets of elements, L1, L2, and L3 that are involved in some of the descriptors in the table above. In the computation of these descriptors, all elements that are not part of the list specified in parenthesis are attributed a weight zero. These lists help build descriptors that characterise the atoms that are more likely to be cause magnetism in a material. Whether an element will induce magnetism in a material is highly dependent on the crystal structure, these lists are thus heuristic. The first list (L1) is the most general. It contains all elements for which one or more of its oxidation states allow magnetism. However, after analyzing the magnetic materials part of the Materials Project database, we notice some elements in L1 nearly never induced magnetism by themselves. In

other words, the materials including these elements and no other element from L1 would rarely be magnetic. The set L2 results from the removal of these elements from L1. The set L3, which is the most uncluttered, was also obtained from L1 by removing elements that are poor inducers of magnetism.

**Elements included in the set L1:** Sc, Ti, V, Cr, Mn, Fe, Co, Ni, Cu, Zr, Nb, Mo, Tc, Ru, Rh, Pd, Ag, Ce, Nd, Pm, Sm, Eu, Gd, Tb, Dy, Ho, Er, Tm, Yb, W, Re, Os, Ir, Pt, Au, U, Np, Pu

**Elements included in the set L2:** Ti, V, Cr, Mn, Fe, Co, Ni, Cu, Nb, Mo, Tc, Ru, Rh, Pd, Ce, Eu, Gd, Tb, W, Re, Os, Ir, U, Np, Pu

**Elements included in the set L3:** V, Cr, Mn, Fe, Co, Ni, Cu, Ru, Ce, Eu, Gd, U, Np, Pu

#### IV. PREDICTIONS ON ICSD

In III, we provide all the references we used to build Tables IV and V in the main text.

Material	Reported magnetic order	Predicted magnetic moment (median)
Eu(NH <sub>2</sub> ) <sub>2</sub>	FM [5]	388 ± 19.04 %
Fe	FM [6]	330 ± 29.12 %
MnS	AFM [7]	282 ± 12.73%
LiFeO <sub>2</sub>	AFM [8]	277 ± 7.73%
LiFe <sub>5</sub> O <sub>8</sub>	AFM [9]	276 ± 24.15%
(NH <sub>4</sub> )MnF <sub>3</sub>	AFM [10]	264 ± 6.83%
LiEuH <sub>3</sub>	FM [11]	257 ± 3.29%
MnF <sub>2</sub>	AFM [12]	255 ± 34.31%
EuH <sub>2</sub>	FM [13]	2539.71%
CaFe <sub>5</sub> O <sub>7</sub>	AFM [14]	251 ± 16.25%
Gd <sub>3</sub> Al	FM [15]	251 ± 0.95%
GdH <sub>2</sub>	AFM [16]	249 ± 0.87%
Mn(OH) <sub>2</sub>	AFM [17]	248 ± 32.28%
Fe <sub>7</sub> SiO <sub>10</sub>	FM [18]	241 ± 22.33%
Fe <sub>3</sub> (PO <sub>4</sub> ) <sub>2</sub> (H <sub>2</sub> O) <sub>8</sub>	AFM [19]	240 ± 33.69%
Y <sub>6</sub> Mn <sub>23</sub> H <sub>26</sub>	AFM [20]	238 ± 25.12%
SrFe <sub>12</sub> O <sub>19</sub>	FM [21]	238 ± 27.32%
MnO(OH)	Other [22]	235 ± 33.15%
Gd	FM [23]	234 ± 10.12%
GdN	FM [24]	234 ± 2.00%
(NH <sub>4</sub> )(MnCl <sub>3</sub> )	AFM [25]	234 ± 5.31%
MnN	FM [26]	233 ± 30.18%
GdMg	FM [27]	233 ± 0.17%
EuO	FM [28]	228 ± 3.84%
Mn <sub>23</sub> Y <sub>6</sub> H <sub>25</sub>	NM [29]	227 ± 24.99%
Fe <sub>15</sub> Co	FM [30]	226 ± 2.04%
Eu	AFM [28]	226 ± 5.52%
Mg(Fe <sub>2</sub> O <sub>4</sub> )	Other [31]	226 ± 19.12%
Gd <sub>6</sub> Mn <sub>23</sub> H <sub>22</sub>	FM [32]	226 ± 12.71%
Fe <sub>16</sub> N <sub>2</sub>	FM [33, 34]	226 ± 3.04%
Fe <sub>7</sub> Co	FM [30]	225 ± 1.94%
Fe <sub>9</sub> Co <sub>7</sub>	FM [30]	225 ± 2.61%
Fe <sub>13</sub> Co <sub>3</sub>	FM [30]	223 ± 1.81%
Fe <sub>5</sub> Co <sub>3</sub>	FM [30]	222 ± 1.81%
Fe <sub>11</sub> Co <sub>5</sub>	FM [30]	222 ± 1.87%
GdB <sub>2</sub>	FM [35]	222 ± 2.16%
Fe <sub>8</sub> N	FM [34]	220 ± 16.82%
CoCo <sub>2</sub> O <sub>4</sub>	FM [36]	220 ± 14.16%
GdO	FM [37]	219 ± 11.96%
Mn <sub>3</sub> N <sub>2</sub>	AFM [38]	215 ± 12.27%
FeCo	FM [30]	215 ± 4.60%
Gd <sub>2</sub> O <sub>3</sub>	Other [39]	213 ± 8.45%
LiEu <sub>4</sub> (BN <sub>2</sub> ) <sub>3</sub>	FM [40]	213 ± 2.90%
Sm <sub>2</sub> Fe <sub>17</sub> N <sub>6</sub>	FM [41]	212 ± 2.53%
EuN	FM [42]	212 ± 3.92%
(H <sub>3</sub> O)Fe <sub>3</sub> (SO <sub>4</sub> ) <sub>2</sub> (OH) <sub>6</sub>	Other [43]	210 ± 30.27%
MnNi	AFM [44]	210 ± 2.59%
Y <sub>6</sub> Mn <sub>23</sub> H <sub>21</sub>	AFM [45]	209 ± 25.13%
GdP	AFM [46]	208 ± 1.83%
CaMn <sub>2</sub> P <sub>2</sub>	AFM [47]	207 ± 34.74%
GdC <sub>2</sub>	AFM [48]	207 ± 0.89%
EuF <sub>2</sub>	PM [49]	205 ± 9.69%
Gd(FeO <sub>3</sub> )	PM [50]	203 ± 14.76%
Y <sub>2</sub> Fe <sub>17</sub> N <sub>3</sub>	FM [51]	203 ± 6.80%
MnSe	AFM [52]	202 ± 5.95%
GdS	AFM [53]	200 ± 3.07%
Y <sub>2</sub> Fe <sub>17</sub> N <sub>2</sub>	FM [54]	197 ± 6.84%
Mn <sub>3</sub> NiN	AFM [55]	197 ± 1.96%
Eu <sub>2</sub> O <sub>3</sub>	NM [56]	197 ± 9.12%
CaMn <sub>7</sub> O <sub>12</sub>	Other [57]	196 ± 14.01%

TABLE III: List of materials used to construct Tables IV and V in the main text.

---

[1] Scikit-learn: Feature importances with a forest of trees, [online], [https://scikit-learn.org/stable/auto\\_examples/ensemble/plot\\_forest\\_importances.html](https://scikit-learn.org/stable/auto_examples/ensemble/plot_forest_importances.html).

[2] Z.-L. Liu, P. Kang, Y. Zhu, L. Liu, and H. Guo, Material informatics for superconductors (2019).

[3] Wolverton Research Group, Magpie, <https://bitbucket.org/wolverton/magpie/src/master/>.

[4] Wikipedia, List of elements by atomic properties (2021).

[5] F. Hulliger, Ferromagnetism of europium amide  $\text{eu}(\text{nh}_2)_2$ , Solid State Communications **8**, 1477 (1970).

[6] J. Crangle and G. M. Goodman, The magnetization of pure iron and nickel, Proceedings of the Royal Society of London. Series A, Mathematical and Physical Sciences **321**, 477 (1971).

[7] J. K. Clark, V. Yannello, A. M. Samarakoon, C. Ross, M. C. Uible, V. O. Garlea, and M. Shatruk, Inelastic neutron scattering study of magnetic exchange pathways in mns, The Journal of Physical Chemistry C **125**, 16183 (2021), <https://doi.org/10.1021/acs.jpcc.1c02956>.

[8] J. Anderson, S. Dey, and V. Halpern, The magnetic susceptibilities of  $\text{lifeo}_2$ , Journal of Physics and Chemistry of Solids **26**, 1555 (1965).

[9] S. Y. An, I.-B. Shim, and C. S. Kim, Synthesis and magnetic properties of  $\text{life}_{508}$  powders by a sol-gel process, Journal of Magnetism and Magnetic Materials **290-291**, 1551 (2005), proceedings of the Joint European Magnetic Symposia (JEMS' 04).

[10] J. Bartolomé, R. Burriel, F. Palacio, D. González, R. Navarro, J. Rojo, and L. De Jongh, Magnetic properties of the weak ferromagnet  $\text{nh}_4\text{mnf}_3$ , Physica B+C **115**, 190 (1983).

[11] J. Greedan, The magnetic properties of  $\text{eulih}_3$ , Journal of Physics and Chemistry of Solids **32**, 819 (1971).

[12] P. Nordblad, L. Lundgren, E. Figueroa, and O. Beckman, Specific heat and magnetic susceptibility of  $\text{mnf}_2$  and  $\text{mn}_{0.98}\text{fe}_{0.02}\text{f}_2$  near  $\text{tn}$ , Journal of Magnetism and Magnetic Materials **23**, 333 (1981).

[13] R. Bischof, E. Kaldas, and P. Wachter, Euh2: A new ferromagnetic semiconductor, Journal of Magnetism and Magnetic Materials **31-34**, 255 (1983).

[14] C. Delacotte, Y. Bréard, V. Caignaert, V. Hardy, J. Grenache, S. Hébert, E. Suard, and D. Pelloquin, Morin-like spin canting in the magnetic  $\text{cafe}_{507}$  ferrite: A combined neutron and mössbauer study, Journal of Solid State Chemistry **247**, 13 (2017).

[15] T. R. McGuire, T. Mizoguchi, R. J. Gambino, and S. Kirkpatrick, Magnetic phase diagram of the gd-al and gd-cu amorphous alloy systems, Journal of Applied Physics **49**, 1689 (1978), <https://doi.org/10.1063/1.324889>.

[16] S. Hémon, R. A. Cowley, R. C. C. Ward, M. R. Wells, L. Douyssset, and H. Ronnow, Magnetic structure of gd,  $\text{gdh}_{2\text{and}}\text{ndh}_{2}$ single crystal films, Journal of Physics: Condensed Matter **12**, 5011–5020 (2000).

[17] A. Christensen and G. Ollivier, Hydrothermal preparation and low temperature magnetic properties of  $\text{mn}(\text{oh})_2$ , Solid State Communications **10**, 609 (1972).

[18] G. Lu, Synthesis of self-assembled iron silicon oxide nanowires onto single-crystalline si(100) (2013), arXiv:1307.7783 [cond-mat.mtrl-sci].

[19] J. B. Forsyth, C. E. Johnson, and C. Wilkinson, The magnetic structure of vivianite,  $\text{fe}_3(\text{po}_4)_2\text{.8h}_2\text{o}$ , Journal of Physics C: Solid State Physics **3**, 1127–1139 (1970).

[20] G. Stewart, J. Zukrowski, and G. Wortmann, Magnetic order in  $\text{y}_6(\text{57fe:mn})_{23}\text{h}_{26}$ , Journal of Magnetism and Magnetic Materials **25**, 77 (1981).

[21] A. Z. Eikeland, M. Stingaciu, A. H. Mamakhel, M. Saura-Múzquiz, and M. Christensen, Enhancement of magnetic properties through morphology control of  $\text{srfe}_{12}\text{o}_{19}$  nanocrystallites, Scientific Reports **8**, 7325 (2018).

[22] L. C. Dong, Y. B. Zhong, S. Zhe, T. Y. Zheng, and H. Wang, Effect of a static magnetic field on the preparation of  $\text{mnooh}$  and  $\text{mn}_3\text{o}_4$  by a hydrothermal process, RSC Adv. **6**, 21037 (2016).

[23] G. V. Brown, Magnetic heat pumping near room temperature, Journal of Applied Physics **47**, 3673 (1976), <https://doi.org/10.1063/1.323176>.

[24] D. X. Li, Y. Haga, H. Shida, T. Suzuki, Y. S. Kwon, and G. Kido, Magnetic properties of stoichiometric gd monopnictides, Journal of Physics: Condensed Matter **9**, 10777–10788 (1997).

[25] R. Burriel, J. Bartolomé, R. Navarro, and D. González, Rotational motion of  $\text{nh}_4+$ in  $\text{nh}_4\text{mncl}_3$  compared to  $\text{nh}_4\text{mnf}_3$ : Heat capacity measurements, in *Recent Developments in Condensed Matter Physics: Volume 4 • Low-Dimensional Systems, Phase Changes, and Experimental Techniques*, edited by J. T. Devreese, L. F. Lemmens, V. E. Van Doren, and J. Van Royen (Springer US, 1981) p. 1–10.

[26] H.-M. Hong, Y.-J. Kang, J. Kang, E.-C. Lee, Y.-H. Kim, and K. J. Chang, Effect of chemical bonding on the magnetic stability and magnetic moment in mn-based binary compounds, Phys. Rev. B **72**, 144408 (2005).

[27] R. Aleonard, P. Morin, J. Pierre, and D. Schmitt, Magnetic properties, magnetic structure of  $\text{gdmg}$  and  $\text{tbmg}$  compounds, Solid State Communications **17**, 599 (1975).

[28] D. B. McWhan, P. C. Souers, and G. Jura, Magnetic and structural properties of europium metal and europium monoxide at high pressure, Phys. Rev. **143**, 385 (1966).

[29] S. Malik, T. Takeshita, and W. Wallace, Hydrogen induced magnetic ordering in  $\text{th}_6\text{mn}_{23}$ , Solid State Communications **23**, 599 (1977).

[30] A. Díaz-Ortiz, R. Drautz, M. Fähnle, H. Dosch, and J. M. Sanchez, Structure and magnetism in bcc-based iron-cobalt alloys, Phys. Rev. B **73**, 224208 (2006).

[31] S. I. Hussein, A. S. Elkady, M. Rashad, A. Mostafa, and R. Megahid, Structural and magnetic properties of magnesium ferrite nanoparticles prepared via edta-based sol-gel reaction, *Journal of Magnetism and Magnetic Materials* **379**, 9 (2015).

[32] F. Pourarian, E. Boltich, W. Wallace, R. Craig, and S. Malik, Magnetic characteristics of r6mn23 hydrides (r = gd, ho or er), *Journal of Magnetism and Magnetic Materials* **21**, 128 (1980).

[33] K. Nakajima, T. Yamashita, M. Takata, and S. Okamoto, Mössbauer study on fe16n2 films prepared by ion-implant nitridation of iron films, *Journal of Applied Physics* **70**, 6033 (1991), <https://doi.org/10.1063/1.350084>.

[34] X. Chen, S. Higashikozono, K. Ito, L. Jin, P.-L. Ho, C.-P. Yu, N.-H. Tai, J. Mayer, R. E. Dunin-Borkowski, T. Suemasu, and X. Zhong, Nanoscale measurement of giant saturation magnetization in a"-fe16n2 by electron energy-loss magnetic chiral dichroism, *Ultramicroscopy* **203**, 37 (2019), 75th Birthday of Christian Colliex, 85th Birthday of Archie Howie, and 75th Birthday of Hannes Lichte / PICO 2019 - Fifth Conference on Frontiers of Aberration Corrected Electron Microscopy.

[35] H. Gencer, T. Izgi, V. S. Kolat, and S. Atalay, Magnetic and magnetocaloric properties of gdb2 compound, *Optoelectronics and Advanced Materials - Rapid Communications* **6**, 875 (2012).

[36] M. A. Rafiq, A. Javed, M. N. Rasul, M. Nadeem, F. Iqbal, and A. Hussain, Structural, electronic, magnetic and optical properties of ab2o4 (a = ge, co and b = ga, co) spinel oxides, *Materials Chemistry and Physics* **257**, 123794 (2021).

[37] T. Yamamoto, K. Kaminaga, D. Saito, D. Oka, and T. Fukumura, Rock salt structure gdo epitaxial thin film with a high ferromagnetic curie temperature, *Applied Physics Letters* **117**, 052402 (2020), <https://doi.org/10.1063/5.0017954>.

[38] A. Leineweber, R. Niewa, H. Jacobs, and W. Kockelmann, The manganese nitrides n-mnn and t-mnn: nuclear and magnetic structures, *Journal of Materials Chemistry* **10**, 2827–2834 (2000).

[39] R. Paul, P. Sen, and I. Das, Effect of morphology on the magnetic properties of gd2o3 nanotubes, *Physica E: Low-dimensional Systems and Nanostructures* **80**, 149 (2016).

[40] M. Somer, C. Güll, R. Müllmann, B. D. Mosel, R. K. Kremer, and R. Pöttgen, Vibrational spectra and magnetic properties of eu3[bn2]2 and lieu4[bn2]3, *Zeitschrift für anorganische und allgemeine Chemie* **630**, 389 (2004), <https://onlinelibrary.wiley.com/doi/pdf/10.1002/zaac.200300366>.

[41] F. Yang, X. Li, J. Wang, Z. Lu, T. Zhao, Q. Li, J. Liu, and F. de Boer, Magnetic properties of sm2fe17ny with al substituted for fe, *Journal of Alloys and Compounds* **221**, 248 (1995).

[42] D. Le Binh, B. J. Ruck, F. Natali, H. Warring, H. J. Trodahl, E.-M. Anton, C. Meyer, L. Ranno, F. Wilhelm, and A. Rogalev, Europium nitride: A novel diluted magnetic semiconductor, *Phys. Rev. Lett.* **111**, 167206 (2013).

[43] W. G. Bisson and A. S. Wills, Anisotropy-driven spin glass transition in the kagome antiferromagnet hydronium jarosite, (h3o)fe3(SO4)2(OH)6, *Journal of Physics: Condensed Matter* **20**, 452204 (2008).

[44] A. Sakuma, Electronic structures and magnetism of cuau-type mnni and mnga, *Journal of Magnetism and Magnetic Materials* **187**, 105 (1998).

[45] A. Kozłowski, G. Stewart, Z. Obuszko, and J. Żukowski, Magnetism in y6mn23hx, *Journal of Magnetism and Magnetic Materials* **92**, 155 (1990).

[46] D. X. Li, Y. Haga, H. Shida, T. Suzuki, and Y. S. Kwon, Electrical transport properties of semimetallic gdx single crystals (x=p, as, sb, and bi), *Phys. Rev. B* **54**, 10483 (1996).

[47] N. S. Sangeetha, S. Pakhira, Q.-P. Ding, L. Krause, H.-C. Lee, V. Smetana, A.-V. Mudring, B. B. Iversen, Y. Furukawa, and D. C. Johnston, First-order antiferromagnetic transitions of srmn2p2 and camn2p2 single crystals containing corrugated-honeycomb mn sublattices, *Proceedings of the National Academy of Sciences* **118**, 10.1073/pnas.2108724118 (2021), <https://www.pnas.org/content/118/44/e2108724118.full.pdf>.

[48] T. Sakai, G. Adachi, and J. Shiokawa, Magnetic properties of the system gdc2-dyc2, *Journal of Applied Physics* **50**, 3592 (1979), <https://doi.org/10.1063/1.326306>.

[49] K. Lee, H. Muir, and E. Catalano, Magnetic and chemical properties of europium fluoride, *Journal of Applied Physics* **36**, 1043 (1965), <https://doi.org/10.1063/1.1714091>.

[50] A. Wu, Z. Wang, B. Wang, X. Ban, L. Jiang, J. Xu, S. Yuan, and S. Cao, Crystal growth and magnetic properties of gdfeo3 crystals by floating zone method, *Solid State Communications* **185**, 14 (2014).

[51] S. Brennan, R. Skomski, O. Cugat, and J. Coey, Anisotropy of easy-plane y2fe17, y2fe17n3 and sm2fe17, *Journal of Magnetism and Magnetic Materials* **140-144**, 971 (1995), international Conference on Magnetism.

[52] R. J. Pollard, V. H. McCann, and J. B. Ward, Magnetic structures of alpha-MnS and MnSe from 57fe mossbauer spectroscopy, *Journal of Physics C: Solid State Physics* **16**, 345 (1983).

[53] U. Kobler, D. Hupfeld, W. Schnelle, K. Mattenberger, and T. Bruckel, Fourth-order exchange interactions in gdeu1-xs, *Journal of Magnetism and Magnetic Materials* **205**, 90–104 (1999).

[54] Y. Yingchang, Z. Xiaodong, K. Linshu, and P. Qi, Magnetic properties of sm2fe17n2 and y2fe17n2, *Chinese Physics Letters* **8**, 318–321 (1991).

[55] M. Wu, C. Wang, Y. Sun, L. Chu, J. Yan, D. Chen, Q. Huang, and J. W. Lynn, Magnetic structure and lattice contraction in mn3nin, *Journal of Applied Physics* **114**, 123902 (2013), <https://doi.org/10.1063/1.4822023>.

[56] C. Wäckerlin, F. Donati, A. Singha, R. Baltic, A.-C. Uldry, B. Delley, S. Rusponi, and J. Dreiser, Strong antiferromagnetic exchange between manganese phthalocyanine and ferromagnetic europium oxide, *Chem. Commun.* **51**, 12958 (2015).

[57] J. Sannigrahi, S. Chattopadhyay, D. Dutta, S. Giri, and S. Majumdar, Magnetic and electric properties of CaMn7o12based multiferroic compounds: effect of electron doping, *Journal of Physics: Condensed Matter* **25**, 246001 (2013).